

Stability and convergence of multi-converter systems using projection-free power-limiting droop control

Amirhossein Iraniparast and Dominic Groß

Abstract—In this paper, we propose a projection-free power-limiting droop control for grid-connected power electronics and an associated constrained flow problem. In contrast to projection-based power-limiting droop control, the novel projection-free power-limiting droop control results in networked dynamics that are semi-globally exponentially stable with respect to the set of optimizers of the constrained flow problem. Under a change to edge coordinates, the overall networked dynamics arising from projection-free power-limiting droop control coincide with the projection-free primal-dual dynamics associated with an augmented Lagrangian of the constrained flow problem. Leveraging this result, we (i) provide a bound on the convergence rate of the projection-free networked dynamics, (ii) propose a tuning method for controller parameters to improve the bound on the convergence rate, and (iii) analyze the relationship of the bound on the convergence rate and connectivity of the network. Finally, the analytical results are illustrated using an Electromagnetic transient (EMT) simulation.

I. INTRODUCTION

The ongoing shift from synchronous machine-based power generation towards power electronics-interfaced generation and energy storage results in significant changes to power system frequency dynamics. Specifically, grid-connected power electronics differ from conventional synchronous generators in terms of their fast response (i.e., milliseconds to seconds) and resource constraints (e.g. power and current limits). Accordingly, incorporating renewable generation resources into large-scale power system challenges standard operating and control paradigm and jeopardizes system stability [1], [2]. For instance, stability analysis of emerging power systems crucially requires considering the constraints of power converters and renewable generation resources such as power limit.

Today, most renewables are interfaced by dc/ac voltage source converters (VSC) use so-called grid-following control. This control paradigm requires a stable and slowly changing ac voltage (i.e., magnitude and frequency) and jeopardizes grid stability when disturbance occur [3]. Since grid-following explicitly controls the converter current/power, incorporating power limits is straightforward. In contrast, grid-forming converters, that are commonly envisioned to be the cornerstone of future power systems, impose stable and self-synchronizing ac voltage dynamics at their grid terminals. Although prevalent

This work was supported in part by the National Science Foundation under Grant No. 2143188. A. Iraniparast and D. Groß are with the Department of Electrical and Computer Engineering at the University of Wisconsin-Madison, USA; e-mail: iraniparast@wisc.edu, dominic.gross@wisc.edu

grid-forming controls including droop control [4], virtual synchronous machine control (VSM) [5], and dispatchable virtual oscillator control (dVOC) [6] have been investigated in detail constraints are not accounted for in their analysis [7]–[11].

However, from a practical point of view, resource and converter constraints are a significant concern. The majority of works on grid-forming control under constraints in the application oriented literature has focused on current-limiting (see [12] for a recent survey). Only few works investigate dc voltage [13] or power limits [14]. Notably, power-limiting droop control combines conventional droop control with proportional-integral controls that activate when the converter reaches its power limit [14].

Continuous-time primal-dual gradient descent dynamics [15] have been widely used to study system-level controls for multi-machine systems such as automatic generation control and economic dispatch [16]. Moreover, primal-dual dynamics have been used to design novel distributed power flow controls [17]. The focus of these works are predominantly equality constrained optimization problems that arise from secondary and tertiary control of power systems.

In contrast, this work leverages projection-free primal-dual dynamics [18] to develop a novel decentralized power-limiting primary control for grid-connected power electronics and analyze the resulting multi-converter system frequency dynamics. Our novel projection-free power-limiting droop control is distinct from power-limiting droop control [14], [19] and enables rigorous bounds on the convergence rate of the multi-converter system frequency to the optimal solution of an associated constrained network flow problem.

Compared with conventional grid-forming droop control [4], power-limiting droop control [14], [19] explicitly accounts for active power limits of resources interfaced by power converters. Moreover, the frequency dynamics of a network of VSCs using power-limiting droop control can be expressed as projected dynamical system [19]. To characterize the steady-states of these networked dynamics, a generic constrained network flow problem can be formulated whose associated primal-dual dynamics are distinct from the networked dynamics and cannot be implemented using only local information [19]. However, leveraging a change of coordinates to edge coordinates [20], the Carathéodory solutions of the projected networked dynamics turn out to be asymptotically stable with respect to Karush-Kuhn-Tucker (KKT) points of the constrained flow problem in edge coordinates. Specifically, in edge coordinates, the primal-dual dynamics associated with the constrained flow problem and the projected networked dynamics coincide. This, enables to represent the networked dynamics a primal-dual

dynamics and apply well-known stability results [15]. Notably, the networked dynamics in nodal coordinates are globally asymptotically stable with respect to the set of optimizers of its associated constrained network problem in nodal coordinates [19]. This result directly establishes frequency stability and synchronization of networks of converters using power-limiting grid-forming droop control. In addition, upon convergence, the converters exhibit power-sharing properties similar to so-called power-sharing in unconstrained droop control [21].

However, the discontinuity of power-limiting droop control hinders convergence analysis and no convergence rate is provided in [19]. In particular, while the stability of the common primal-dual gradient descent is well-studied as a discontinuous dynamical (e.g., [15]), well-known results do not provide a convergence rate. However, from a practical point of view, bounds on the convergence rate are crucial for, e.g., tuning controls and analyzing performance. To address this challenge, continuous primal-dual dynamics associated with an augmented Lagrangian have been introduced that are exponentially stable and admit rigorous bounds on the convergence rate [18], [22].

Our main contribution is to leverage the projection-free primal-dual dynamics [22] to develop a novel projection-free power-limiting droop control, establish semi-global exponential stability of the resulting networked multi-converter frequency dynamics with respect to KKT points of an associated constrained flow problem, obtain a bound on the convergence rate of the networked multi-converter dynamics, and analyze the impact of control gains and network parameters on the convergence rate.

In particular, our projection-free power-limiting droop control results in projection-free networked dynamics whose Carathéodory solutions are semi-globally exponentially stable with respect to KKT points of the constrained flow problem introduced in [19]. To obtain this result, we show that the projection-free networked dynamics corresponds to the primal-dual dynamics of the constrained network flow problem in edge coordinates. Therefore, all existing results on the properties of the KKT points of the constrained flow problem (e.g., synchronous frequency) and steady states of projection-based power-limiting droop control [19] immediately hold for the proposed projection-free power-limiting droop control.

A key contribution of this work is a bound on the convergence rate of the projection-free networked dynamics. To this end, we characterize the active constraint set and graph of nodes with active constraints. Notably, to evaluate the convergence rate of the resulting projection-free power-limiting droop control, we link the Jacobian matrix of the constraints of the network flow problem to the Laplacian matrix of the graph of nodes with active constraints. This result enables bounding the convergence rate of the networked dynamics as a function of the control gains and properties of the network (e.g., connectivity, maximum node degree, edge weights). In turn, this allows us to propose a control tuning that improve the bound on the convergence rate. In addition, we show that, under mild technical assumptions, the bound on the convergence rate can be improved by adding edges (e.g., transmission lines) to the graph that increase the connectivity

of the graph. Finally, an Electromagnetic transient (EMT) simulation of the IEEE 9-bus system is used to illustrate the results and validate that the proposed control tuning improves control performance.

Notation

We use \mathbb{R} and \mathbb{N} to denote the set of real and natural numbers and define, e.g., $\mathbb{R}_{\geq 0} := \{x \in \mathbb{R} | x \geq 0\}$. Moreover, we use $\mathbb{S}_{>0}^n$ and $\mathbb{S}_{\geq 0}^n$ to denote the set of real positive definite and positive semidefinite matrices. For column vectors $x \in \mathbb{R}^n$ and $y \in \mathbb{R}^m$ we define $(x, y) = [x^T, y^T]^T \in \mathbb{R}^{n+m}$. Moreover, $\|x\| = \sqrt{x^T x}$ denotes the Euclidean norm and $\|x\|_C := \min_{z \in C} \|z - x\|$ denotes the point to set distance. Furthermore, I_n , $\mathbb{0}_{n \times m}$, $\mathbb{0}_n$, and $\mathbb{1}_n$ denote the n -dimensional identity matrix, $n \times m$ zero matrix, and column vectors of zeros and ones of length n respectively. The cardinality of a discrete set \mathcal{X} is denoted by $|\mathcal{X}|$. The Kronecker product is denoted by \otimes . We use $\varphi_x(t, x_0)$ to denote a (Caratheodory) solution of $\frac{d}{dt}x = f(x)$ at time $t \in \mathbb{R}_{\geq 0}$ starting from x_0 at time $t = 0$.

II. NETWORK MODEL AND PRELIMINARIES

In this section, we introduce the ac power network model, converter model, and converter control that will be considered throughout the paper.

A. Power network and converter model in nodal coordinates and control objectives

Consider an ac power network modeled by a simple, connected and undirected graph $\mathcal{G} := \{\mathcal{N}, \mathcal{E}, \mathcal{W}\}$ with edge set $\mathcal{E} := \mathcal{N} \times \mathcal{N}$ corresponding to $|\mathcal{E}| = e$ transmission lines, set of nodes \mathcal{N} corresponding to $|\mathcal{N}| = n$ voltage source converters, and set of edge weights $\mathcal{W} = \{w_1, \dots, w_e\}$ with $w_i \in \mathbb{R}_{>0}$ for all $i \in \{1, \dots, e\}$ modeling transmission line susceptances [23]. Throughout this work, we assume that the network is lossless, and modeled through a Kron-reduced graph. Moreover, we model each voltage source converter $i \in \mathcal{N}$ as a voltage source imposing an ac voltage with phase angle $\theta_i \in \mathbb{R}$ that injects an active power denoted by $P_i \in \mathbb{R}$. Finally, for every $i \in \mathcal{N}$, we use $P_{L,i} \in \mathbb{R}$ to denote active power loads mapped from the load nodes (i.e., nodes eliminated by applying Kron reduction) to the converter nodes.

Linearizing the ac power flow equation at the nominal voltage magnitude and zero angle difference between nodes, results in the converter power injection

$$P := L\theta + P_L, \quad (1)$$

where $L := BWB^T$ is the Laplacian matrix of the graph \mathcal{G} , $B \in \{-1, 0, 1\}^{n \times e}$ denotes the oriented incidence matrix of \mathcal{G} , and $W = \text{diag}\{w_i\}_{i=1}^e$. Moreover, $\theta = (\theta_1, \dots, \theta_n) \in \mathbb{R}^n$ is the vector of ac voltage phase angles (relative to $\omega_0 t$ with nominal frequency $\omega_0 \in \mathbb{R}_{>0}$), $P_L := (P_{L,1}, \dots, P_{L,n}) \in \mathbb{R}^n$ is the vector of active power loads at every node, and $P = (P_1, \dots, P_n) \in \mathbb{R}^n$ is the vector of converter power injections. Our objective is to design a (decentralized) feedback controller that maps the converter power injection P_i to the frequency

$\omega_i = \frac{d}{dt}\theta_i$ to control the power system to the solution of constrained flow problem (CFP) given by

$$\min_{\theta, P} \quad \frac{1}{2} \|P - P^*\|_M^2 \quad \text{s.t.} \quad P_\ell \leq L\theta + P_L \leq P_u \quad (2)$$

where $M := \text{diag}\{m_i\}_{i=1}^n \in \mathbb{S}_{>0}^n$ is a diagonal matrix of droop gains, $P^* := (P_1^*, \dots, P_n^*) \in \mathbb{R}^n$ is a vector of local references, and $P_\ell := (P_{\ell,1}, \dots, P_{\ell,n}) \in \mathbb{R}^n$ and $P_u := (P_{u,1}, \dots, P_{u,n}) \in \mathbb{R}^n$ model limits on the network injections. The following assumptions ensure feasibility of (3).

Assumption 1 (Feasible injection limits and loads) For all $i \in \mathcal{N}$, the limits $P_{\ell,i} \in \mathbb{R}^n$ and $P_{u,i} \in \mathbb{R}^n$ satisfy $P_{\ell,i} < P_{u,i}$. Moreover, the disturbance input $P_L \in \mathbb{R}^n$ satisfies $\sum_{i=1}^n P_{\ell,i} < \sum_{i=1}^n P_{L,i} < \sum_{i=1}^n P_{u,i}$.

Assumption 2 (Feasible references) The setpoints $P_i^* \in \mathbb{R}^n$ satisfy $P_{\ell,i} < P_i^* < P_{u,i}$.

The next proposition ensures feasibility of the CFP (3) under Assumption 1.

Proposition 1 (Feasibility in nodal coordinates [19]) There exists $\theta \in \mathbb{R}^n$ such that $P_\ell < L\theta + P_L < P_u$ if and only if P_ℓ , P_u , and P_L satisfy Assumption 1.

Finally, we define S_θ as the set of KKT points of (1) (for details see [19, Def. 1]). Moreover, let $K_I := \text{diag}\{\sqrt{k_{I,i}}\}_{i=1}^n \in \mathbb{S}_{>0}^n$ denote a diagonal matrix scaling the constraints. The set of KKT points of

$$\min_{\theta} \quad \frac{1}{2} \|L\theta\|_M^2 + (P_L - P^*)^\top M L \theta \quad (3a)$$

$$\text{s.t.} \quad K_I P_\ell \leq K_I (L\theta + P_L) \leq K_I P_u \quad (3b)$$

is identical to S_θ [19].

B. Power network and converter model in edge coordinates

Using the oriented incidence matrix B and $V := W^{\frac{1}{2}} \in \mathbb{R}^{n \times n}$, we define the change of coordinates $\eta = VB^\top \theta$ as the so-called edge coordinates [20]. The power injection (1) in edge coordinates follows

$$P := BV\eta + P_L. \quad (4)$$

Next, consider the constrained flow problem in edge coordinates

$$\min_{\eta} \quad \frac{1}{2} \|BV\eta\|_M^2 + (P_L - P^*)^\top MBV\eta \quad (5a)$$

$$\text{s.t.} \quad K_I P_\ell \leq K_I (BV\eta + P_L) \leq K_I P_u. \quad (5b)$$

Assumption 3 The linear independence constraint qualification (LICQ) holds at any optimizer η^* of (5).

Finally, we define S_η as the set of KKT points of (4) (for details see [19, Def. 8]).

C. Graph of nodes with active constraints

Using the following definitions, we introduce the active constraint graph associated with \mathcal{G} .

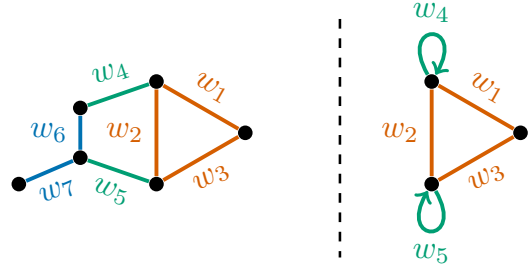


Fig. 1: The graph \mathcal{G} and the active graph \mathcal{G}_I corresponding to \mathcal{I}_I : inactive constraint nodes (blue), active constraint nodes (red), edges connecting active constraint nodes (orange), and edges connecting active and inactive constraint nodes (green).

Definition 1 (Active constraint sets) We define $\mathcal{I}_\ell \subseteq \mathcal{N}$ and $\mathcal{I}_u \subseteq \mathcal{N} \setminus \mathcal{I}_\ell$ as the set of nodes at their lower and upper limit, i.e., $i \in \mathcal{I}_\ell$ if and only if $P_i = P_{\ell,i}$ and $i \in \mathcal{I}_u$ if and only if $P_i = P_{u,i}$. Moreover, we define $\mathcal{I} := \mathcal{I}_\ell \cup \mathcal{I}_u$.

Definition 2 (Graph of nodes with active constraint) Let B_I contain the rows of B associated with the active set \mathcal{I} . Moreover, we define the graph \mathcal{G}_I containing nodes $i \in \mathcal{I}$ and edges $(i, j) \in (\mathcal{I} \times \mathcal{I}) \cap \mathcal{E}$. Additionally, edges connecting nodes $i \in \mathcal{I}$ and nodes $j \notin \mathcal{I}$ appear as self-loops in \mathcal{G}_I .

By extracting the weights corresponding to active nodes as W_I , we define the Laplacian matrix associated with \mathcal{G}_I as $L_I = B_I W_I B_I^\top$, where removing the rows of B corresponding to inactive nodes results in B_I with (i) fully zero columns associated with edges of the inactive part of the graph, (ii) columns containing only 1 or -1 associated with edges connecting the inactive part of the graph to that of the active part and (iii) columns containing 1 and -1 associated with edges of the active part of the graph. It should be noted that the edges connecting the inactive to the active part of the graph represent themselves as self-loops in L_I (see Fig. 1).

Now we can discuss the relation between the Laplacian L_I and the Jacobian of the CFP constraints in edge coordinates. Let \mathcal{J} denote the Jacobian of the constraints (5b). At any optimizer η^* of (5), we define

$$\kappa := \lambda_{\min}(\mathcal{J}_{\mathcal{I}_\ell \cup \mathcal{I}_u} \mathcal{J}_{\mathcal{I}_\ell \cup \mathcal{I}_u}^\top),$$

where \mathcal{J}_I contains the row vectors of the Jacobian \mathcal{J} whose indices are in \mathcal{I} . Moreover, Assumption 3 implies that $\kappa > 0$. As shown in the next proposition κ is equivalent to the minimum eigenvalue of the Laplacian L_I scaled with the controller gains K_{I_ℓ} of the inactive nodes.

Proposition 2 For any diagonal matrix $K_{I_\ell} \in \mathbb{S}_{>0}^n$ and Laplacian L_I , it holds that $\kappa = \lambda_{\min}(K_{I_\ell} L_I K_{I_\ell})$.

Proof. Suppose that $\mathcal{I}_\ell \cup \mathcal{I}_u = \mathcal{I}$, since we have $\mathcal{J}_I = (K_I B)_I = K_{I_\ell} B_I V_I$, then by the definition of κ , and Definition 2, it immediately follows that $\kappa = \lambda_{\min}(K_{I_\ell} B_I V_I V_I^\top B_I^\top K_{I_\ell})$ and $\kappa = \lambda_{\min}(K_{I_\ell} L_I K_{I_\ell})$. \square

It follows from [19, Proposition 2] that either $\mathcal{I}_\ell = \emptyset$ or $\mathcal{I}_u = \emptyset$. This immediately results in the following corollary.

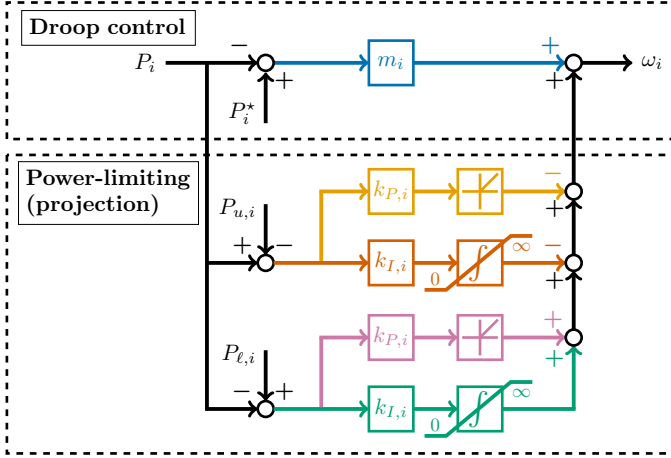


Fig. 2: Projection-based power-limiting droop control

Corollary 1 It holds that either $\kappa = \lambda_{\min}(\mathcal{J}_{\mathcal{I}_\ell} \mathcal{J}_{\mathcal{I}_\ell}^\top)$ or $\kappa = \lambda_{\min}(\mathcal{J}_{\mathcal{I}_u} \mathcal{J}_{\mathcal{I}_u}^\top)$. Moreover, for uniform controller gains, i.e., $k_{I,i} = c \in \mathbb{R}_{>0}$ for all $i \in \mathcal{N}$, it holds that $\kappa = c \lambda_{\min}(L_{\mathcal{I}})$.

III. PROJECTION-FREE POWER LIMITING DROOP CONTROL

In this section, we first review results for (projection-based) power-limiting droop control [14], [19]. Then we introduce the novel projection-free power-limiting droop control.

A. Review of projection-based network dynamics

Computing the optimal solution of (3) via its associated primal-dual dynamics [15] results in a distributed algorithm that requires exchanging dual-multipliers between nodes. This is not feasible on primary frequency control timescales in large-scale power systems. In contrast, the projection-based network dynamics depicted in Fig. 2, that resemble but are distinct from the well-known primal-dual dynamics, solve (3) using only local information [19]. We require the following definition of projection operator to formalize the projection-based and projection-free network dynamics.

Definition 3 (Projection) Given a convex set $\mathcal{C} \subseteq \mathbb{R}^n$ and a vector $v \in \mathbb{R}^n$, $\Pi_{\mathcal{C}}(v)$ denotes the projection of v with respect to the set \mathcal{C} , i.e., $\Pi_{\mathcal{C}}(v) = \operatorname{argmin}_{p \in \mathcal{C}} \|p - v\|$.

Next, consider the projection-based power-limiting droop control with states $\frac{d}{dt}\theta_i = \omega_i$, $\lambda_{u,i} \in \mathbb{R}_{\geq 0}$, and $\lambda_{\ell,i} \in \mathbb{R}_{\geq 0}$ that correspond to the ac voltage phase angles and integral of the upper and lower power limit violations (see Fig. 2). Let

$$g(P_N) = \begin{bmatrix} g_\ell(P_N) \\ g_u(P_N) \end{bmatrix} := \begin{bmatrix} P_\ell - P_N - P_L \\ P_N + P_L - P_u \end{bmatrix}.$$

The interconnection of the nodal dynamics in Fig. 2 via (1) can be written as the projected dynamical system

$$\begin{aligned} \frac{d}{dt}\theta &= M(P^* - P_L - L\theta) - (\Xi \otimes K_I)\lambda \quad (6a) \\ &\quad - (\Xi \otimes K_P)\Pi_{\mathbb{R}_{\geq 0}^{2n}}(g(L\theta)), \end{aligned}$$

$$\frac{d}{dt}\lambda = \Pi_{\mathcal{T}_\lambda \mathbb{R}_{\geq 0}^{2n}}((I_2 \otimes K_I)g(L\theta)), \quad (6b)$$

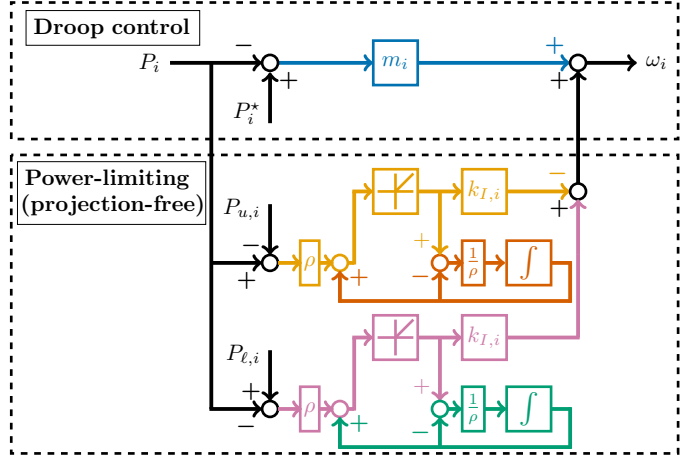


Fig. 3: Projection-free power-limiting droop control

where $\Xi := (-1, 1)^\top$ and $\lambda := (\lambda_\ell, \lambda_u) \in \mathbb{R}_{\geq 0}^{2n}$ collects the integrator states. Moreover, the matrix $K_P := \operatorname{diag}\{k_{P,i}\}_{i=1}^n$ collects proportional gains $k_{P,i} \in \mathbb{R}_{>0}$. We emphasize that this model assumes that the load P_L , power setpoints P^* , and power limits P_ℓ and P_u are constant on the time-scales of interest for studying frequency stability.

While multi-converter network dynamics (6) do not coincide with the primal-dual dynamics of (3) in nodal coordinates, they coincide after transformation to edge coordinates. Notably, using $\eta = VB^\top\theta$ to transform the multi-converter network dynamics (6) results in dynamics that coincide with the primal-dual dynamics of the CFP (5) in edge coordinates (see [19, Fig. 1]). Building upon this observation and the LaSalle function from [15], it can be shown that (6) converges to optimal (i.e., KKT) points of (3) [19]. However, this analysis does not provide a convergence rate. In addition, due to the discontinuity of the dual dynamics, the projection-based network dynamics (6) cannot converge exponentially [22].

In the next section, we introduce the projection-free networked dynamics that are the main focus of this paper.

B. Projection-free networked dynamics

To overcome these conceptual limitations of projection-based power-limiting droop control, we introduce the novel projection-free power-limiting droop control (see Fig. 3)

$$\begin{aligned} \frac{d}{dt}\theta_i &= m_i(P_i^* - P_i) - k_{I,i}\Pi_{\mathbb{R}_{\geq 0}}(\rho(P_i - P_{u,i}) + \lambda_{u,i}) \quad (7a) \\ &\quad + k_{I,i}\Pi_{\mathbb{R}_{\geq 0}}(\rho(P_{\ell,i} - P_i) + \lambda_{\ell,i}), \end{aligned}$$

$$\frac{d}{dt}\lambda_{\ell,i} = \frac{1}{\rho}(\Pi_{\mathbb{R}_{\geq 0}}(\rho(P_{\ell,i} - P_i) + \lambda_{\ell,i}) - \lambda_{\ell,i}), \quad (7b)$$

$$\frac{d}{dt}\lambda_{u,i} = \frac{1}{\rho}(\Pi_{\mathbb{R}_{\geq 0}}(\rho(P_i - P_{u,i}) + \lambda_{u,i}) - \lambda_{u,i}). \quad (7c)$$

This controller is motivated by the projection-free primal-dual dynamics introduced in [18], [22]. The remainder of this manuscript analyzes the interconnection of the nodal dynamics (7) via (1) given by

$$\frac{d}{dt}\theta = M(P^* - L\theta - P_L) - (\Xi \otimes K_I)\Pi_{\mathbb{R}_{\geq 0}^{2n}}(\rho g(L\theta) + \lambda), \quad (8a)$$

$$\rho \frac{d}{dt}\lambda = \Pi_{\mathbb{R}_{\geq 0}^{2n}}(\rho g(L\theta) + \lambda) - \lambda. \quad (8b)$$

We emphasize that the projection-free multi-converter frequency dynamics (8) do not coincide with the projection-free primal-dual dynamics associated with the CFP (3) in nodal coordinates. However, applying the change of coordinates to edge coordinates, the projection-free multi-converter frequency dynamics coincide with the projection-free primal-dual dynamics of (5). Thus, [22, Theorem 1] can be used to establish exponentially convergence of the multi-converter frequency dynamics to KKT points of (3) and bound the convergence rate.

IV. STABILITY OF PROJECTION-FREE NETWORKED DYNAMICS IN EDGE COORDINATE

The Augmented Lagrangian introduced in [24] associated with the CFP in edge coordinates (5) is given by

$$\begin{aligned} \mathcal{L}(\eta, \mu_\ell, \mu_u) = & \frac{1}{2} \|BV\eta\|_M^2 + (P_L - P^*)^\top MBV\eta \\ & + \sum_{j=1}^m \mathcal{H}_\rho(-a_j^\top \eta - b_j, \mu_{j,\ell}) + \mathcal{H}_\rho(a_j^\top \eta - c_j, \mu_{j,u}) \end{aligned} \quad (9)$$

with penalty function

$$\begin{aligned} \mathcal{H}_\rho(a_j^\top \eta - b_j, \mu_j) = & \begin{cases} (a_j^\top \eta - b_j)\mu_j + \frac{\rho}{2}(a_j^\top \eta - b_j)^2 & \text{if } \rho(a_j^\top \eta - b_j) + \mu_j \geq 0 \\ -\frac{1}{2}\frac{\mu_j^2}{\rho} & \text{if } \rho(a_j^\top \eta - b_j) + \mu_j < 0 \end{cases} \end{aligned}$$

Here, a_j is the j -th column of $(K_I BV)^\top$, b_j is the j -th element of $K_I(P_L - P_\ell)$, c_j is the j -th element of $K_I(P_u - P_L)$, and $\mu_\ell \in \mathbb{R}_{\geq 0}$ and $\mu_u \in \mathbb{R}_{\geq 0}$ are the dual multipliers associated with the lower and upper inequalities respectively.

Note that $\sum_{j=1}^n x_j \Pi_{\mathbb{R}_{\geq 0}^n}(y_j) = X^\top \Pi_{\mathbb{R}_{\geq 0}^n}(y)$, where x_j is the j -th column of matrix X and y_j is the j -th element of the column vector y . Then, primal-dual gradient dynamics associated with (9) are given by $\mu = (\mu_\ell, \mu_u)$ and

$$\frac{d}{dt}\eta = VB^\top \left(M(P^* - P_L - BV\eta) \right) \quad (11a)$$

$$- (\Xi \otimes K_I) \Pi_{\mathbb{R}_{\geq 0}^{2n}} (\rho(I_2 \otimes K_I) g(BV\eta) + \mu) \quad (11b)$$

$$\rho \frac{d}{dt}\mu = \Pi_{\mathbb{R}_{\geq 0}^{2n}} (\rho(I_2 \otimes K_I) g(BV\eta) + \mu) - \mu. \quad (11b)$$

The next theorem establishes the projection-free networked dynamics (8) and projection-free primal-dual dynamics (11) coincide in edge coordinates. To this end, let $T_\eta := \text{blkdiag}(VB^\top, K_I)$.

Theorem 1 (Coinciding dynamics) Consider any initial condition (θ_0, λ_0) of the projection-free networked dynamics (8) in nodal coordinates. Moreover, consider the corresponding initial condition $(\eta_0, \mu_0) = T_\eta(\theta_0, \lambda_0)$ of the projection-free primal-dual dynamics (11) of (9) in edge coordinates. Then, the solutions $\varphi_\theta(t, (\theta_0, \lambda_0))$ and $\varphi_\eta(t, (\eta_0, \mu_0))$ of (8) and (11) satisfy $T_\eta \varphi_\theta(t, (\theta_0, \lambda_0)) = \varphi_\eta(t, T_\eta(\theta_0, \lambda_0))$.

Proof. Using the change of variables $\mu = K_I \lambda$ and [19, Lemma 2], the networked dynamics (8) can be written as

$$\frac{d}{dt}\theta = M(P^* - L\theta - P_L) \quad (12a)$$

$$- (\Xi \otimes K_I) \Pi_{\mathbb{R}_{\geq 0}^{2n}} (\rho(I_2 \otimes K_I) g(L\theta) + \mu) \quad (12a)$$

$$\rho \frac{d}{dt}\mu = \Pi_{\mathbb{R}_{\geq 0}^{2n}} (\rho(I_2 \otimes K_I) g(L\theta) + \mu) - \mu \quad (12b)$$

Recalling the definition $g(P_N)$ and using edge coordinate $\eta = VB^\top \theta$, the network dynamics in edge coordinates become identical to (11). Moreover, since $\frac{d}{dt}\eta \in \text{Im } VB^\top$ holds for (11a) and any initial condition $\eta_0 \in \text{Im } VB^\top$, it holds that $\eta \in \text{Im } VB^\top$ for all $t \in \mathbb{R}_{\geq 0}$. For any initial condition (θ_0, μ_0) trajectories of (12) mapped to the edge coordinates coincide with trajectories of (11) with the initial condition $(VB^\top \theta_0, \mu_0)$. We conclude that the projection-free networked dynamics (7) mapped to edge coordinate coincide with the primal-dual dynamics associated with (9) for any initial condition $\eta_0 \in \text{Im}(VB^\top)$. \square

Before establishing stability of the network dynamics in edge coordinate (11), we need to extend the definition of semi-global exponential stability [25, Theorem 5.17] to semi-global exponential stability with respect to a set.

Definition 4 (Semi-global exponential stability) Consider the autonomous dynamical system $\frac{d}{dt}z(t) = \phi(z(t))$ and its set \mathcal{Z}_e of equilibrium points. Any point $z_e \in \mathcal{Z}_e$ is a semi-global exponentially equilibrium point, if for any $h > 0$, there exist $\mathcal{M}_\beta > 0$ and $\beta > 0$ such that for any initial point z_0 such that $\|z_0\|_{\mathcal{Z}_e} \leq h$, the corresponding solution $z(t)$ of the dynamical system satisfies

$$\|z(t)\|_{\mathcal{Z}_e} \leq \mathcal{M}_\beta \cdot e^{-\beta t} \|z(0)\|_{\mathcal{Z}_e}, \quad \forall t \in [0, \infty].$$

Although Definition 4 does not require any properties on the set of equilibrium points, in our analysis \mathcal{Z}_e is a convex set of points satisfying KKT conditions.

The next proposition states bounds for the maximum eigenvalue of Laplacian L .

Proposition 3 Consider the degree d_i of node $i \in \mathcal{N}$, the minimum and maximum edge weights w_{\min} and w_{\max} , and maximum node degree $d_{\max} := \max_{i \in \mathcal{N}} d_i$. Then, the largest eigenvalue of the Laplacian L is bounded by

$$w_{\min}(1 + d_{\max}) \leq \lambda_{\max}(L) \leq 2w_{\max}d_{\max}. \quad (13)$$

A proof is provided in the Appendix. We are now ready to state our main stability result.

Theorem 2 (Semi-global exponential stability of primal-dual dynamics in edge coordinates) Consider P_ℓ , P_u , P_L , and P^* such that Assumption 1 and Assumption 2 hold. Then, under Assumption 3, the primal-dual dynamics (11) are semi-globally exponentially stable with respect to \mathcal{S}_η on $\mathbb{R}^e \times \mathbb{R}_{\geq 0}^{2n}$. Moreover, $\frac{d}{dt}(\eta, \lambda) = \mathbb{0}_{e+2n}$ holds on \mathcal{S}_η .

A proof is provided in the Appendix.

We emphasize that the frequency and active constraints upon convergence for both projection-based and projection-free power limiting droop control are identical and solely determined by the KKT points of (3). In particular, synchronous frequency ω_s can be explicitly expressed as a function of the active sets \mathcal{I}_u and \mathcal{I}_ℓ , total load $\sum_{i \in \mathcal{N}} P_{L,i}$, total power dispatch $\sum_{i \in \mathcal{N}} P_i^*$, and droop coefficients [19, Th. 3].

V. CONVERGENCE RATE

In this section, before addressing the convergence rate, we study the stability of the proposed networked dynamics in nodal coordinates.

A. Preliminaries

Proposition 4 (Semi-global exponential stability of networked dynamics in nodal coordinates) Consider P_ℓ , P_u , P_L , and P^* such that Assumption 1 and Assumption 2 hold. For any connected graph \mathcal{G} , (8) is semi-globally exponentially stable on $\mathbb{R}^n \times \mathbb{R}_{\geq 0}^{2n}$ with respect to the set \mathcal{S}_θ . Moreover, there exists $\omega_s \in \mathbb{R}$ such that $\lim_{t \rightarrow \infty} \omega_i(t) = \omega_s$ for all $i \in \mathcal{N}$.

Proof. Definition 4 does not restrict the initial condition and we consider nonnegative initial values $\lambda(0), \mu(0) \geq 0$. In this case, the dual multipliers remain in nonnegative orthant [22, Proposition 1]. Next, we can establish the stability of the dynamical system in original coordinates. Notably, there exist $\underline{\kappa} \in \mathbb{R}_{\geq 0}$ and $\bar{\kappa} \in \mathbb{R}_{\geq 0}$, $\forall t \geq 0$ such that

$$\underline{\kappa} \|T_\eta \varphi_\theta(t, \xi_0)\|_{\mathcal{S}_\theta} \leq \|\varphi_\theta(t, \xi_0)\|_{\mathcal{S}_\theta} \leq \bar{\kappa} \|T_\eta \varphi_\theta(t, \xi_0)\|_{\mathcal{S}_\theta} \quad (14)$$

By [19, Theorem 1], it follows that the left inequality holds with $\underline{\kappa} = \|T_\eta\|^{-1}$. Next, let $\sigma_1 := \min_{\theta \perp \mathbb{1}_n, \|\theta\|=1} \|VB^\top \theta\| \in \mathbb{R}_{>0}$. Then, the upper bound of (14) holds with $\bar{\kappa} = \frac{1}{\min\{1, \sigma_1\}}$. By Theorem 2, (11) is semi-globally exponentially stable on $\mathbb{R}^e \times \mathbb{R}_{\geq 0}^{2n}$ with respect to \mathcal{S}_η . Using Theorem 2 and the upper bound of (14), we have

$$\|\varphi_\eta(t, T_\eta \xi_0)\|_{\mathcal{S}_\eta} \leq \mathcal{M}_\beta \cdot e^{-\beta t} \|\varphi_\eta(0, T_\eta \xi_0)\|_{\mathcal{S}_\eta}$$

where $\|\varphi_\theta(t, \xi_0)\|_{\mathcal{S}_\theta} \leq \bar{\kappa} \|\varphi_\eta(t, T_\eta \xi_0)\|_{\mathcal{S}_\eta}$ and \mathcal{M}_β is a constant depending on the decaying rate β . Moreover, we have $\|\varphi_\eta(0, T_\eta \xi_0)\|_{\mathcal{S}_\eta} \leq \underline{\kappa}^{-1} \|\varphi_\theta(0, \xi_0)\|_{\mathcal{S}_\theta}$. Finally, we conclude

$$\|\varphi_\theta(t, \xi_0)\|_{\mathcal{S}_\theta} \leq \bar{\kappa} \cdot \underline{\kappa}^{-1} \cdot \mathcal{M}_\beta \cdot e^{-\beta t} \|\varphi_\theta(0, \xi_0)\|_{\mathcal{S}_\theta}.$$

In other words, (7) is semi-globally exponentially stable on $\mathbb{R}^n \times \mathbb{R}_{\geq 0}^{2n}$ with respect to the set \mathcal{S}_θ . In addition, we show that $\lim_{t \rightarrow \infty} \omega(t) = \mathbb{1}_n \omega_s$. According to Theorem 2, any pair (η^*, λ^*) converges to a KKT point $(\eta^*, \lambda^*) \in \mathcal{S}_\eta$, i.e., $\lim_{t \rightarrow \infty} \eta(t) = \eta^*$ and $\lim_{t \rightarrow \infty} \frac{d}{dt} \eta = \mathbb{0}_e$. Using $\eta = VB^\top \theta$, we obtain

$$\lim_{t \rightarrow \infty} \frac{d}{dt} VB^\top \theta(t) = \lim_{t \rightarrow \infty} VB^\top \frac{d}{dt} \theta(t) = \lim_{t \rightarrow \infty} VB^\top \omega(t) = 0$$

and $\lim_{t \rightarrow \infty} \omega(t) = \mathbb{1}_n \omega_s$ follows $\ker(B^\top) = \text{span}(\mathbb{1}_n)$ to conclude the proof. \square

B. Convergence rate

Next, using results for the primal-dual gradient dynamics associated with the augmented Lagrangian [15], [22], globally asymptotic stability of the projection-free networked dynamics in nodal coordinate (7) can be established. However, since the gradient of the constraints (5b), i.e., BV is not full row rank, a global exponential convergence rate cannot be obtained [26]. We begin by introducing several constants that are needed to establish semi-global exponential convergence of the projection-free networked dynamics.

First, let M_g denote an upper bound on the spectral norms of the Jacobian \mathcal{J} given by the maximum control gain $k_{I,\max} := \max_{i \in \mathcal{N}} k_{I,i}$, $M_g = \sqrt{2k_{I,\max} w_{\max} d_{\max}}$ (see Prop. 3), and

$$\|K_I BV\|_2 \leq \|K_I\|_2 \|BV\|_2 \leq \sqrt{k_{I,\max} \lambda_{\max}(L_e)} \quad (15a)$$

$$\leq \sqrt{k_{I,\max} \lambda_{\max}(L)} \leq M_g. \quad (15b)$$

Next, let L_g denote an upper bounds on the Frobenius norms of the Jacobian \mathcal{J} of the constraint (5b) given by

$$\|K_I BV\|_F \leq \|K_I\|_2 \|B\|_2 \|V\|_F \quad (16a)$$

$$\leq \sqrt{2d_{\max} k_{I,\max} w_\Sigma} = L_g \quad (16b)$$

where we used $w_\Sigma := \sum_{j=1}^e w_j$, $\|B\|_2 = \sqrt{\|B\|_1 \|B\|_\infty}$, $\|B\|_\infty = d_{\max}$, and $\|B\|_1 = 2$. Using M_g and L_g , we define

$$\mathcal{M}_\theta(\rho, L_g, M_g) = \rho L_g^2 + M_g(\rho L_g d_0 + d_0 + \|\mu^*\|). \quad (17)$$

Moreover, we define the edge Laplacian associated with the Laplacian L as $L_e = VB^\top BV$, then we have

$$m_{\min} \lambda_{\max}(L_e) \leq \lambda_{\max}(VB^\top MBV) \leq m_{\max} \lambda_{\max}(L_e).$$

Using $\lambda_{\max}(L_e) = \lambda_{\max}(L)$ [20] and Proposition 3, $\gamma = \lambda_{\max}(VB^\top MBV)$, we have

$$m_{\min} w_{\min}(1 + d_{\max}) \leq \gamma \leq 2m_{\max} w_{\max} d_{\max}.$$

Finally, we require α -strong convexity of (5a) and γ -lipschitzness of its gradient. To this end, note that

$$\lambda_{\min}(\Gamma_+^\top VB^\top MBV \Gamma_+) = \lambda_{\min}^+(VB^\top MBV)$$

In addition,

$$m_{\min} \lambda_{\min}^+(L) \leq \lambda_{\min}^+(VB^\top MBV)$$

where $\lambda_{\min}^+(L)$ is the algebraic connectivity of the graph \mathcal{G} . Thus, we conclude that¹

$$0 < \underline{\alpha} \leq \alpha \leq \gamma \leq \bar{\gamma}$$

with $\underline{\alpha} = m_{\min} \lambda_{\min}^+(L)$ and $\bar{\gamma} = 2w_{\max} m_{\max} d_{\max}$.

Next, recall the conditions on the convergence rate β [22]

$$\beta \leq \frac{\kappa \delta_{\min}}{46 \rho L_g^2}, \quad (22a)$$

$$\frac{\kappa \alpha}{4\beta} - 4\beta^2 \geq L_g^2 + \frac{\kappa}{4} + (\gamma + \mathcal{M}_\theta)(\alpha + \mathcal{M}_\theta + \frac{1}{\rho}) + \frac{1}{2\rho^2}. \quad (22b)$$

Moreover, we define

$$\delta_{\min}(\rho, k_{I,i}) := 1 - \left[1 + \rho \cdot \frac{\max_{i \in N \setminus (\mathcal{I}_u \cup \mathcal{I}_\ell)} \sqrt{k_{I,i}} g_i(\eta^*)}{d_0} \right]_+,$$

where $d_0 \in \mathbb{R}_{>0}$ is the point to set distance of initial primal-dual pair $(\eta_0, \mu_{\ell,0}, \mu_{u,0})$ to the set of KKT points \mathcal{S}_η .

We can now state the following corollary that establishes semi-global exponential convergence of the projection-free networked dynamics.

Corollary 2 Let $\beta \in \mathbb{R}_{>0}$ denote any strictly positive constant satisfying (22). Then, there exists $\mathcal{M}_\beta \in \mathbb{R}_{>0}$ such that $\lim_{\beta \rightarrow 0^+} \mathcal{M}_\beta = 1$ and

$$\|\varphi_\theta(t, \xi_0)\|_{\mathcal{S}_\theta} \leq \bar{\kappa} \cdot \underline{\kappa}^{-1} \cdot \mathcal{M}_\beta \cdot e^{-\beta t} \|\varphi_\theta(0, \xi_0)\|_{\mathcal{S}_\theta}.$$

The corollary directly follows from [22, Theorem 1].

¹This bound holds for any graph \mathcal{G} with $n \geq 3$. Moreover, for $n = 2$ the second-smallest eigenvalue can be obtained explicitly.

C. Control tuning

Although the bounds in Corollary 2 explicitly depend on ρ , changing the controller gains implicitly manipulate the boundaries by changing the other parameters. Accordingly, it is crucial to address how to choose the controller gains to improve the closed-loop convergence rate. To this end, the next proposition introduces the idea to manipulate the given gain ρ and controller gains k_i to enlarge the boundaries.

Proposition 5 Consider controller gains $k_{I,i} \in \mathbb{R}_{>0}$ and $\rho \in \mathbb{R}_{>0}$. Moreover, let $k'_i = sk_{I,i}$ and $\rho' = \frac{1}{\sqrt{s}}\rho$. For all $s \in \mathbb{R}_{>1}$, it holds that

$$\beta(k_{I,i}, \rho) < \beta(k'_i, \rho').$$

Proof. Let $\zeta_\beta = \frac{\alpha}{\beta} - \frac{16\beta^2}{\kappa}$, $\zeta_1 = \frac{4L_g^2}{\kappa}$, and $\zeta_2 = \frac{4}{\kappa}((\gamma + \mathcal{M}_\theta)(\alpha + \mathcal{M}_\theta + \frac{1}{\rho}) + \frac{1}{2\rho^2})$. Under the conditions of Corollary 2, it holds that

$$\zeta_\beta \geq \zeta_1 + \zeta_2 + 1.$$

Notably, ζ_β is an increasing function with respect to κ , i.e., $\frac{\partial \zeta_\beta}{\partial \kappa} = \frac{16\beta^2}{\kappa^2} > 0$. Scaling the gains $k'_{I,i} = sk_{I,i}$, we obtain $L'_g = \sqrt{s}\kappa L_g$, $\kappa' = s\kappa$ and $M'_g = \sqrt{s}M_g$ respectively. In other words, ζ_β increases and $\frac{\partial \zeta_1}{\partial s} = \frac{\partial}{\partial s} \frac{4L_g^2}{\kappa'^2} = 0$. Therefore, it is sufficient to show that ζ_2 decreases under scaling by s . Expanding ζ_2 results in

$$\zeta_2 = 4\left(\frac{\gamma\alpha}{\kappa} + \frac{(\gamma + \alpha)M_\theta}{\kappa} + \frac{\gamma}{\kappa\rho} + \frac{M_\theta(M_\theta + \frac{1}{\rho})}{\kappa} + \frac{1}{2\kappa\rho^2}\right).$$

Note that $\frac{\partial}{\partial s} \frac{\gamma\alpha}{\kappa'} < 0$ and $\frac{\partial}{\partial s} \frac{\gamma}{\kappa'\rho'} < 0$, i.e., the first and third term decrease as s increases. Moreover, the last term is unchanged since $\frac{\partial}{\partial s} \frac{1}{\kappa'\rho'^2} = 0$. Next, we show that the second term of ζ_2 decreases and the fourth term of ζ_2 is unchanged as s increases. For brevity consider $M'_\theta = M_\theta(\rho', L'_g, M'_g)$ resulting in

$$\frac{\partial}{\partial s} \frac{M'_\theta}{\kappa'} = \frac{\partial}{\partial s} \frac{\rho(L_g^2 + L_g M_g d_0)}{\sqrt{s}\kappa} + \frac{\partial}{\partial s} \frac{M_g(d_0 + \|\mu^*\|)}{\sqrt{s}\kappa} < 0.$$

Additionally, for the fourth term

$$\begin{aligned} \frac{\partial}{\partial s} \frac{M_\theta^2}{\kappa'} &= \frac{\partial}{\partial s} \frac{\rho^2(L_g^2 + M_g L_g d_0)^2}{\kappa} \\ &+ \frac{\partial}{\partial s} \frac{M_g^2(d_0 + \|\mu^*\|)^2}{\kappa} \\ &+ \frac{\partial}{\partial s} \frac{2\rho(L_g^2 + M_g L_g d_0)M_g(d_0 + \|\mu^*\|)}{\kappa} = 0 \end{aligned}$$

and

$$\begin{aligned} \frac{\partial}{\partial s} \frac{M'_\theta}{\kappa'\rho'} &= \frac{\partial}{\partial s} \frac{\rho L_g^2 + M_g(\rho L_g d_0 + d_0 + \|\mu^*\|)}{\kappa\rho} \\ &= \frac{\partial}{\partial s} \frac{L_g^2}{\kappa} + \frac{\partial}{\partial s} \frac{M_g L_g d_0}{\kappa} + \frac{\partial}{\partial s} \frac{M_g(d_0 + \|\mu^*\|)}{\kappa\rho} \\ &= 0. \end{aligned}$$

We conclude that $\frac{\kappa\alpha}{4\beta} - 4\beta^2$ increases for any increasing $s > 1$, i.e., $\frac{\partial \zeta_2}{\partial s} < 0$. Moreover, recalling $\beta \leq \frac{\kappa\delta_{\min}}{46\rho L_g^2}$ and the

definition of δ_{\min} we have

$$\delta_{\min}(\rho, k_{I,i}) := 1 - \left[1 + \rho \cdot \frac{\max_{i \in N \setminus (\mathcal{I}_u \cup \mathcal{I}_\ell)} \sqrt{k_{I,i}} g_i(\eta^*)}{d_0} \right]_+^2.$$

This implies that $\frac{\partial}{\partial s} \frac{\kappa' \delta_{\min}(\rho', k'_{I,i})}{46\rho' L_g^2} = \frac{\partial}{\partial s} \frac{\sqrt{s}\kappa \delta_{\min}(\rho, k_{I,i})}{46\rho L_g^2} > 0$. Due to enlargement of both bounds on β in Corollary 2, irrespective of the dependency of M_β on β , we conclude that $\beta(k_{I,i}, \rho) < \beta(k'_i, \rho')$. \square

This result establishes that the convergence rate increases for increasing $s \in \mathbb{R}_{>1}$, i.e., increasing $k_{I,i}$ and decreasing ρ according to Proposition 5. Next, we bound the maximum achievable convergence rate.

Proposition 6 The maximum convergence rate β_{\max} is bounded by $\min\{\frac{\kappa\delta_{\min}}{46\rho L_g^2}, \tilde{c}\} \leq \beta_{\max} \leq \frac{1}{46\rho}$, where $\tilde{c} = \sqrt[3]{\frac{-q}{2} + \sqrt{\frac{q^2}{4} + \frac{p^3}{27}}} + \sqrt[3]{\frac{-q}{2} - \sqrt{\frac{q^2}{4} + \frac{p^3}{27}}}$, $c = \frac{5}{4}L_g^2 + (\bar{\gamma} + \mathcal{M}_\theta)(\bar{\gamma} + \mathcal{M}_\theta + \frac{1}{\rho}) + \frac{1}{2\rho^2}$, $p = \frac{c}{4}$, and $q = -\frac{\kappa\alpha}{16}$.

Proof. By the definition of κ , it holds that $\kappa < L_g^2$. Since $\delta_{\min} \leq 1$, this results in the upper bound. Solving (22b) resulting from the second inequality in Corollary 2 results in the lower bound. \square

This result establishes that the upper bound on the maximum achievable convergence rate β_{\max} increases as the gain ρ decreases. On the other hand, the lower bound on the maximum achievable convergence rate β_{\max} has a non-trivial dependence on both the controller gains and network topology.

Finally, we bound the gains ρ to narrows down the range of gains ρ to be considered for controller tuning.

Proposition 7 The gain ρ^* corresponding to the maximum convergence rate β in Corollary 2 is bounded by

$$\frac{2c_1}{23\kappa\alpha} < \rho^* \leq 1 + \frac{1}{23\kappa\alpha} \max\{2c_1, 2\gamma, \frac{1062}{1058}\}.$$

Proof. Since $\frac{\kappa\alpha}{4\beta} - 4\beta^2$ is a decreasing function of β , any ρ that satisfy the conditions of Corollary 2 satisfies

$$\frac{23}{2}\kappa\alpha\rho^3 - c_1\rho^2 - \gamma\rho - \frac{531}{1058} > 0$$

where $c_1 = L_g^2 + \frac{\kappa}{4} + \gamma\alpha$. Therefore, since $\gamma\rho + \frac{531}{1058} > 0$ we have $\frac{23}{2}\kappa\alpha\rho^3 > c_1\rho^2$ and $\rho > \frac{2c_1}{23\kappa\alpha}$. Moreover, an upper bound on the solution is given by

$$\rho \leq 1 + \frac{1}{23\kappa\alpha} \max\{2c_1, 2\gamma, \frac{1062}{1058}\}$$

The result follows from feasibility of the optimum ρ^* . \square

D. Impact of network topology

In addition to the control gains, the convergence rate of the projection-free networked dynamics crucially depends on the network topology and edge weights (e.g., transmission line susceptances). In this section, we analyze the impact of key network parameters on the convergence rate.

To this end, recall that d_i , $i \in \mathcal{N}$, and d_{\max} denotes the node degree and maximum node degree. The following proposition

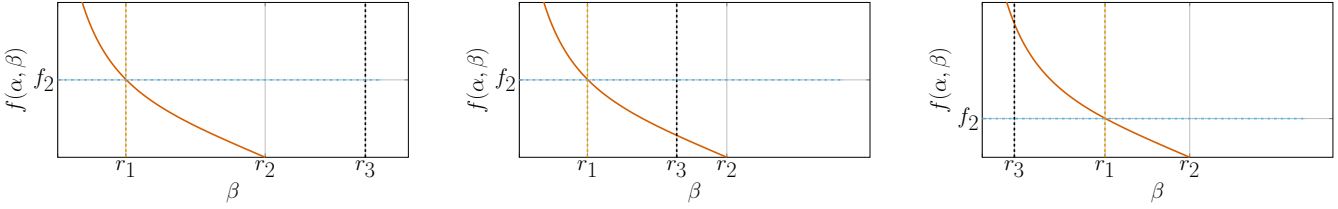


Fig. 4: Representative different cases of bounds (22a) and (22b) indicating the decaying rate β , $f(\alpha, \beta)$ and f_2 are left and righthand side of the bound (22b) respectively, where $r_1 = \arg_\beta(f(\alpha, \beta) = f_2)$, $r_2 = \sqrt[3]{\frac{\kappa C}{16}}$, and $r_3 = \frac{\kappa \delta_{\min}}{46\rho L_g^2}$.

establishes that, under some technical assumptions, the convergence rate β increases when the connectivity of the graph \mathcal{G} increases.

Proposition 8 Consider adding an edge with weight $w_{e+1} \leq w_{\max}$ between any two nodes $(i, j) \notin \mathcal{E}$ that satisfy $d_l < d_{\max}$, $l \in i, j$. Then, $\beta(\rho, k_{I,i})$ remains unchanged if (22a) is binding. On the other hand, $\beta(\rho, k_{I,i})$ increases if (22b) is binding and $\rho \in \mathbb{R}_{>0}$ satisfies

$$\left(\frac{21}{2} - cd_0\right)\rho \geq \frac{m_{\max}}{k_{i,\max}}c^2 + \frac{d_0 + \|\mu^*\|}{\sqrt{2k_{i,\max}d_{\max}w_{\Sigma}}}c$$

with $c = \sqrt{\frac{w_{\max}}{w_{\Sigma}}}$.

Proof. Adding the edge (i, j) between these nodes increases the connectivity $\lambda_{\min}^+(L)$. In turn, this results in increased α . Let $f(\alpha, \beta) := \frac{\kappa\alpha}{4\beta} - 4\beta^2$, and $f_2 = L_g^2 + \frac{\kappa}{4} + (\gamma + M_\theta)(\alpha + M_\theta + \frac{1}{\rho}) + \frac{1}{2\rho^2}$. Then, (22b) can be written as $f(\alpha, \beta) \geq f_2$. Moreover, $f(\alpha, \beta) \geq f_2$ is satisfied for all $\beta \leq \min\{\frac{\kappa\delta_{\min}}{46L_g^2}, \arg_\beta(f(\alpha, \beta) = f_2)\}$. Taking the derivative of $f(\alpha, \beta) \geq f_2$ with respect to α and rearranging the resulting inequality results in

$$\beta \leq \frac{\kappa}{4(\gamma + M_\theta)}.$$

Thus, if (22a) is binding, then $\beta(\rho, k_{I,i})$ is unchanged. Otherwise, (22b) is binding if $\frac{\kappa}{4(\gamma + M_\theta)} \leq \frac{\kappa\delta_{\min}}{46L_g^2}$. This results in

$$46\rho L_g^2 \geq \delta_{\min} 4(\gamma + M_\theta).$$

Since $\delta_{\min} \leq 1$ it is sufficient to show

$$46\rho L_g^2 \geq 4(\gamma + \rho L_g^2 + M_g(\rho L_g d_0 + d_0 + \|\mu^*\|)).$$

For this inequality to hold, ρ has to satisfy

$$(1 - \frac{2}{21} \frac{M_g}{L_g} d_0) \rho \geq \frac{2}{21} \frac{\gamma}{L_g^2} + \frac{2}{21} \frac{M_g}{L_g^2} (d_0 + \|\mu^*\|).$$

In addition, $\frac{\gamma}{L_g^2} \leq \frac{m_{\max}w_{\max}}{k_{I,\max}w_{\Sigma}}$, $\frac{M_g}{L_g^2} = \frac{\sqrt{w_{\max}}}{\sqrt{k_{I,\max}d_{\max}w_{\Sigma}}}$, and $\frac{M_g}{L_g} d_0 = \sqrt{\frac{w_{\max}}{w_{\Sigma}}} d_0$. \square

This results shows that, under mild technical assumptions, adding edges that connect previously weakly connected nodes (i.e., increasing the connectivity of the network) increases the convergence rate of the projection-free networked dynamics. Specifically, on a sufficiently large gain ρ , the convergence rate can be improved by introducing an edge with a weight equal or lower than w_{\max} connecting any two nodes with degree less than d_{\max} .

Moreover, the following corollary establishes the same result for the simpler setup of a graph with identical weights.

Corollary 3 Consider a graph \mathcal{G} with uniform edge weights $w_i = w'$ for all $i \in \{1, \dots, e\}$ and let $k_{i,\max} = s_m m_{\max}$ denote the controller gain as function of the maximum droop gain m_{\max} and $s_m \in \mathbb{R}_{>1}$. For any connected graph \mathcal{G} with $n \geq 3$ the lower bound on ρ in Proposition 8 can be replaced by

$$(21e - 2\sqrt{e}d_0)\rho \geq \frac{2}{s_m} + \frac{d_0 + \|\mu^*\|}{\sqrt{k_{i,\max}w'}}$$
(23)

where e is the number of edges.

Corollary 3 shows that, as long as the number of edges e and distance d_0 of the initial primal-dual pair satisfy $21e - 2\sqrt{e}d_0 > 0$, increasing the number of edges e improves the bound on ρ for which Prop. 8 holds. In other words, adding edges as outlined in Prop. 8 improves the convergence rate for lower gains ρ if the initial number of edges e is larger.

VI. NUMERICAL CASE STUDY

To illustrate and validate our analytical results obtained for the reduced-order model (7) and (1) of the frequency dynamics of multi-converter power systems, we use an electromagnetic transient (EMT) simulation of the IEEE 9-bus system (see Fig. 5) with three VSCs controlled by power limiting droop control.

A. Power system model

Specifically, we replaced the three synchronous generators in the IEEE 9-bus system with voltage source converters (VSCs). An average model of two-level VSCs with LC output filter and standard cascaded inner voltage and current loops is used. Details on the transformer parameters, converter parameters, and control gains of the inner control loops can be found in [27]. Table I and [19, Table I] summarize the converter rating, power setpoints, power limits, and control gains for power-limiting droop control used in this work. In addition to the standard IEEE 9-bus base load a time-varying constant power load (see Fig. 5) is introduced to create overload conditions for the VSCs. Notably, the reduced-order model (7) is obtained by applying kron-reduced [23] to obtain a network model with three buses and assuming that active power and frequency are decoupled from reactive power and voltage magnitude.

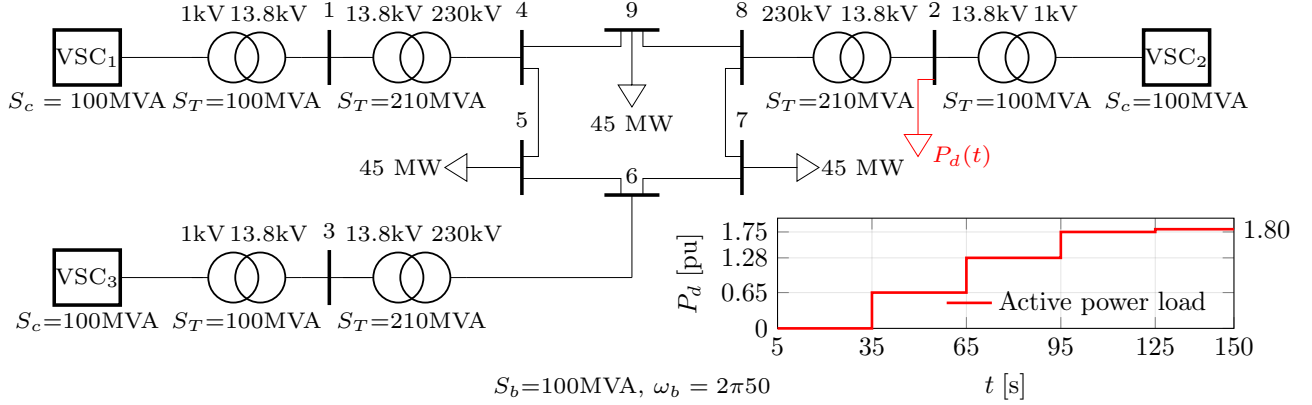


Fig. 5: IEEE 9-bus test case system with three two-level voltage source converters and constant impedance (black) and constant power loads (red).

B. Simulation results and discussion

Simulation results are shown in Fig. 6 and Fig. 7. EMT simulation results are shown in the top row and simulation results obtained using the reduced-order model (7) are shown in the bottom row. The pink markers in the bottom row of Fig. 6 indicate the frequency deviation predicted by [19, Theorem 3]. Under the same load profile used in [19], we validate the analytical results for the synchronous frequency, and observe that the analytical results closely match the EMT simulation and results obtained using the reduced-order model (7).

Finally, to compare projection-based [19] and projection-free power-limiting droop control (7) the response of active power to a load increase and subsequent convergence are shown in Fig. 7. Notably, before the load increase at $t = 95$ s, VSC 2 is overloaded. In addition, the load increase at $t = 95$ s overloads VSC 3. Moreover, after the load increase at $t = 125$ s all VSCs operate at their maximum active power. In addition, we validate the improvement of the convergence rate according to Proposition 5 by scaling controller gains, i.e., using the scaling $s = 1.66$ improves the convergence rate relative to using the scaling $s = 1$.

TABLE I: Model and control parameters. For further details see [27, Table I].

VSC	Power [MW]			Control gains [pu]		
	P^*	P_ℓ	P_u	m_p	ρ	k_I
1	25 MW	20 MW	110 MW	4.17%	1.02	40.95
2	87.5 MW	20 MW	110 MW	9.38%	1.02	40.95
3	55 MW	20 MW	110 MW	6%	1.02	40.95

VII. APPENDIX

Proof of Proposition 3. The Laplacian L associated with the undirected graph \mathcal{G} is defined as

$$L_{i,j} = \begin{cases} \sum_k w_{(i,k)}, & i = j, (i,k) \in \mathcal{E}, \\ -w_{(i,j)}, & i \neq j, (i,j) \in \mathcal{E}, \\ 0, & \text{otherwise.} \end{cases}$$

Since $\mathbb{1}_n \in \ker(L)$, the sum of absolute value of off-diagonal terms of each row of the Laplacian L is equal to its corresponding diagonal term. Thus Gershgorin's circle theorem implies that the eigenvalues of the Laplacian are located in a union of the closed discs, i.e., $\lambda_i \in \bigcup_{i=1}^n \mathbb{D}(\sum_k w_{(i,k)}, \sum_k w_{(i,k)})$. Next, let $w_{\Sigma,i} = \sum_k w_{(i,k)}$ and note that

$$\mathbb{D}(w_{\Sigma,i}, w_{\Sigma,i}) \subseteq \mathbb{D}(\max_i(w_{\Sigma,i}), \max_i(w_{\Sigma,i})).$$

Thus, using $\max_i(\sum_k w_{(i,k)}) \leq w_{\max} d_{\max}$, the upper bound is obtained. To establish the lower bound, note that $\lambda_{\max}(L) \geq w_{\min} \lambda_{\max}(B^T B)$. It suffices to show that $\lambda_{\max}(B^T B) \geq 1 + d_{\max}$. To this end, by the Rayleigh quotient, we have

$$\lambda_{\max}(B^T B) \geq x^T B^T B x \quad \forall \|x\| = 1$$

where $x^T B^T B x = \sum_{(i,j) \in \mathcal{E}} (x_i - x_j)^2$. Next, let $\Delta := \frac{1}{\sqrt{d_{\max}^2 + d_{\max}}}$ and $x = \Delta [d_{\max} \ -1 \ \dots \ -1 \ 0 \ \dots \ 0]$. The Proposition follows by noting that x has d_{\max} number of elements equal to $-\Delta$ and $n - d_{\max} - 1$ of zero elements. \square

Proof of Theorem 2. We begin by noting that $M \in \mathbb{S}_{\geq 0}^n$. Then, by [28, Observation 7.1.8], $B^T M B \in \mathbb{S}_{\geq 0}^{e \times e}$ if and only if $\text{rank } B = e$. If \mathcal{G} is a connected tree, then $n = e + 1$ and by [29, Lem. 9.2], $\text{rank } B = e$. Conversely, if \mathcal{G} contains cycles, then $e \geq n$ and $\text{rank } B \leq e - 1$. Thus, if \mathcal{G} is a tree, then the cost function of (5) is strongly convex and \mathcal{S}_η is a singleton. Moreover, by [19, Prop. 3] there exists η such that $P_\ell < BV\eta + P_L < P_u$, i.e., Slater's condition holds. Then, by Assumption 3, [22, Thm. 1] immediately implies that (11) is semi-globally exponentially stable with respect to \mathcal{S}_η .

When \mathcal{G} contains cycles, we can decompose (5) into a strongly convex part and convex part. Similarly, the dynamics (11) can be decomposed into an semi-globally exponentially stable part and Lyapunov stable part. To this end, let $\Gamma := [\Gamma_+ \ \Gamma_0]$ where $\Gamma_+ \in \mathbb{R}^{e \times n-1}$ contains eigenvectors corresponding to the positive eigenvalues of $VB^T M B V$ and $\Gamma_0 \in \mathbb{R}^{e \times e-(n-1)}$ contains the eigenvectors corresponding to the zero eigenvalues. Next, let $\gamma = (\gamma_+, \gamma_0) \in \mathbb{R}^e$. Since $B^T M B \in \mathbb{S}_{\geq 0}^n$, we conclude that $\Gamma^{-1} = \Gamma^T$. Applying the

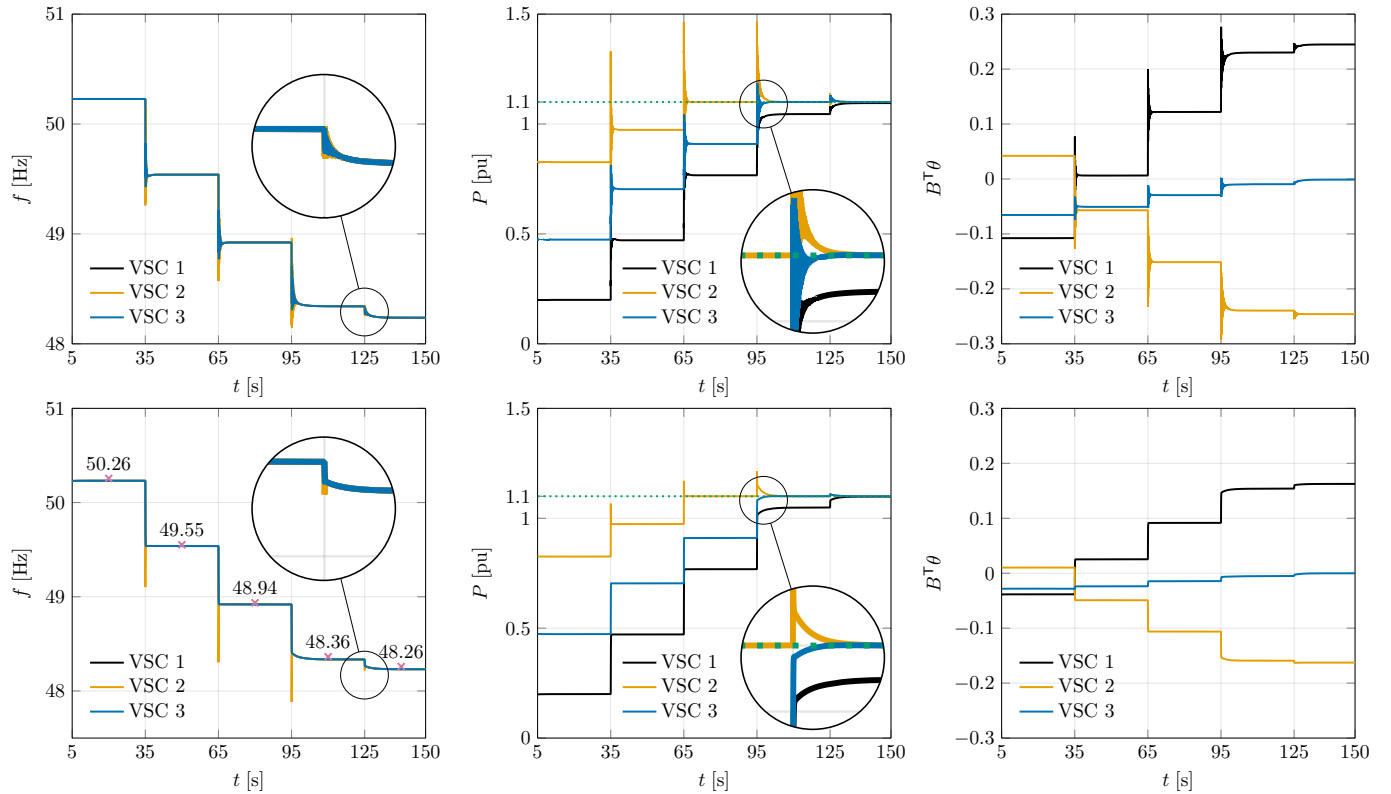


Fig. 6: Results of an EMT simulation (top row) and the reduced-order model (bottom row) for the IEEE 9-bus system depicted in [19, Fig. 3.]. The green line indicates the upper power limit of each VSC and the pink markers indicate the frequency deviation predicted by [19, Theorem 3] using the parameters in [19, Table I].

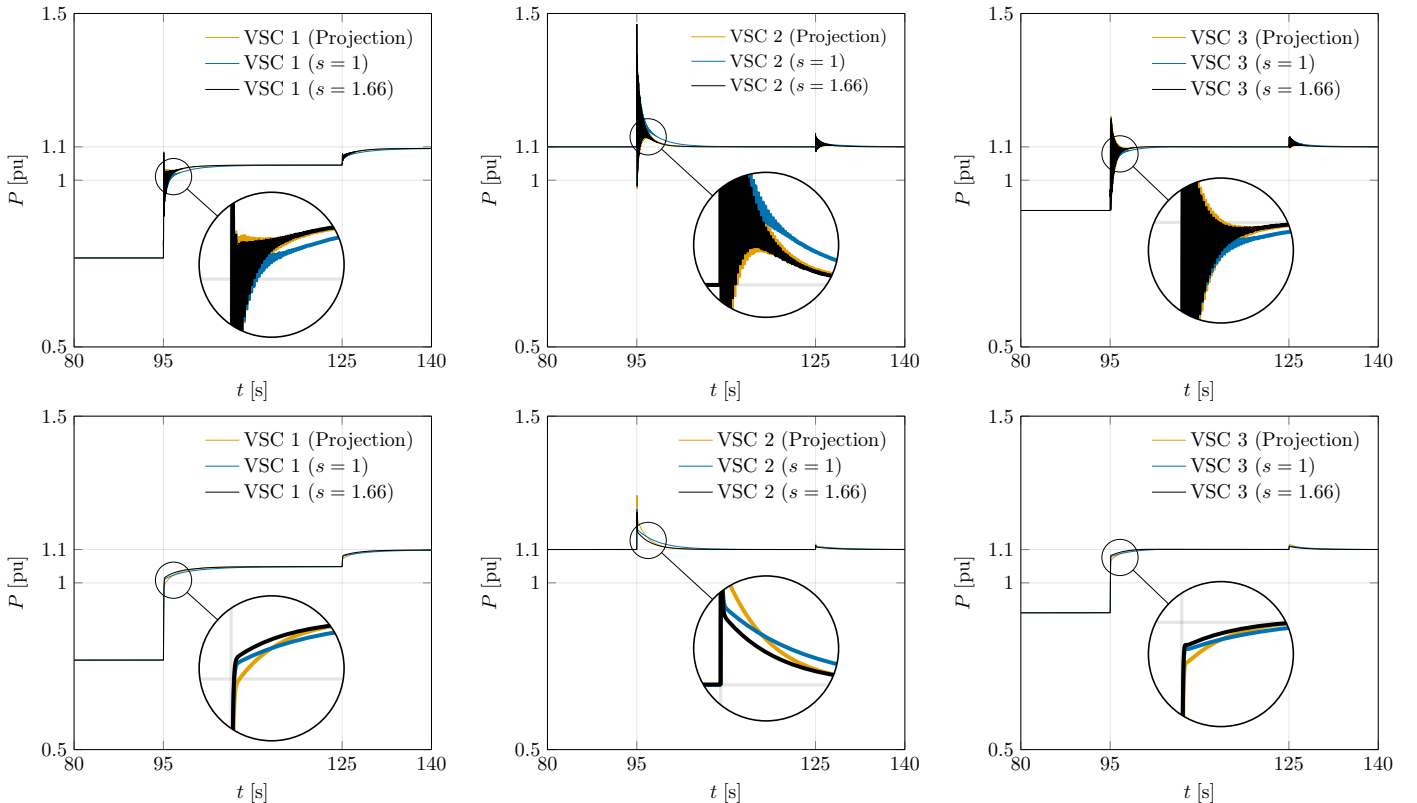


Fig. 7: Comparison of an EMT simulation (top row) and the reduced-order model (bottom row) of the IEEE 9-bus using the projection-based and projection-free dynamics for different values of scaling factor s .

change of coordinates $\eta = \Gamma\gamma$ to (5) results in

$$\min_{\gamma_+} \frac{1}{2} \|\gamma_+\|_H^2 + c^\top \gamma_+ \quad (24a)$$

$$\text{s.t. } K_I \ell \leq K_I(A\gamma_+ + P_L) \leq K_I P_u, \quad (24b)$$

where $H := \Gamma_+^\top V B^\top M B V \Gamma_+$, $c := \Gamma_+^\top V B M (P^* - P_L)$, and $A := B V \Gamma_+$. Notably, this transformation only removed redundant degrees of freedom and, by construction, (24) is strongly convex and strictly feasible under the same conditions as (5). Moreover, given a KKT point (γ_+^*, λ^*) of (24), $B V \Gamma_0 \in \mathbb{R}^{n \times e-(n-1)}$ implies that $(\Gamma_+ \gamma_+^* + \Gamma_0 \gamma_0, \lambda^*) \in \mathcal{S}_\eta$ for all $\gamma_0 \in \mathbb{R}^{e-(n-1)}$. Applying the change of coordinates $\eta = \Gamma\gamma$ to (11) results in $\frac{d}{dt}\gamma_0 = 0$ and

$$\begin{aligned} \frac{d}{dt}\gamma_+ &= -H\gamma_+ - c - (K_I A)^\top (\Pi_{\mathbb{R}_{\geq 0}^n}(\rho K_I g_1(A\gamma_+) + \mu_\ell) \\ &\quad + \Pi_{\mathbb{R}_{\geq 0}^n}(\rho K_I g_2(A\gamma_+) + \mu_u)), \end{aligned} \quad (25a)$$

$$\frac{d}{dt}\mu_\ell = \frac{1}{\rho}(\Pi_{\mathbb{R}_{\geq 0}^n}(\rho K_I g_\ell(A\gamma_+) + \mu_\ell) - \mu_\ell), \quad (25b)$$

$$\frac{d}{dt}\mu_u = \frac{1}{\rho}(\Pi_{\mathbb{R}_{\geq 0}^n}(\rho K_I g_u(A\gamma_+) + \mu_u) - \mu_u). \quad (25c)$$

Notably, (25) corresponds to primal-dual dynamics associated with the augmented Lagrangian of (24). Thus, by [22, Theorem 1], the dynamics (25) are semi-globally exponentially stable with respect to a KKT point (γ_+^*, λ^*) of (24). In other words, (11) can be decomposed into dynamics that are semi-globally exponentially stable with respect to (γ_+^*, λ^*) and a constant $\gamma_0 \in \mathbb{R}^{e \times e-(n-1)}$. Since $(\eta, \lambda) = (\Gamma_+ \gamma_+ + \Gamma_0 \gamma_0, \lambda) \in \mathcal{S}_\eta$ for any γ_0 , it follows that (11) is semi-globally exponentially stable with respect to \mathcal{S}_η . The last statement of the Theorem follows by noting that $\frac{d}{dt}(\gamma_+, \lambda) = \mathbb{0}_{3n-1}$ when $(\gamma_+, \lambda) = (\gamma_+^*, \lambda^*)$ and $\frac{d}{dt}\gamma_0 = 0$. Moreover, (i) by the invariance subspace principle, LICQ is inherited from (5) since the transformation Γ is invertible, (ii) there exist upper bounds on the Frobenius and spectral norm of the Jacobian matrix of the constraints, and (iii) when \mathcal{G} is a tree, (5) is strongly convex, and if \mathcal{G} is not a tree, then (24) is strongly convex. Finally, using Proposition 3, (15b), and (16b) concludes the proof. \square

REFERENCES

- [1] B. Kroposki, B. Johnson, Y. Zhang, V. Gevorgian, P. Denholm, B.-M. Hodge, and B. Hannegan, “Achieving a 100% renewable grid: Operating electric power systems with extremely high levels of variable renewable energy,” *IEEE Power and Energy Magazine*, vol. 15, no. 2, pp. 61–73, 2017.
- [2] F. Milano, F. Dörfler, G. Hug, D. J. Hill, and G. Verbić, “Foundations and challenges of low-inertia systems (invited paper),” in *Power Systems Computation Conference*, 2018.
- [3] B. Kroposki and A. Hoke, “A path to 100 percent renewable energy: Grid-forming inverters will give us the grid we need now,” *IEEE Spectrum*, vol. 61, no. 5, pp. 50–57, 2024.
- [4] M. Chandorkar, D. Divan, and R. Adapa, “Control of parallel connected inverters in standalone ac supply systems,” *IEEE Trans. Ind. Appl.*, vol. 29, no. 1, pp. 136–143, 1993.
- [5] S. DÁRCO, J. A. Suul, and O. B. Fosso, “A virtual synchronous machine implementation for distributed control of power converters in smartgrids,” *Electric Power Systems Research*, vol. 122, pp. 180–197, 2015.
- [6] D. Groß, M. Colombino, J.-S. Brouillon, and F. Dörfler, “The effect of transmission-line dynamics on grid-forming dispatchable virtual oscillator control,” *IEEE Transactions on Control of Network Systems*, vol. 6, no. 3, pp. 1148–1160, 2019.
- [7] F. Dörfler and F. Bullo, “Synchronization and transient stability in power networks and nonuniform kuramoto oscillators,” *SIAM Journal on Control and Optimization*, vol. 50, no. 3, pp. 1616–1642, 2012.
- [8] J. Schiffer, R. Ortega, A. Astolfi, J. Raisch, and T. Sezi, “Conditions for stability of droop-controlled inverter-based microgrids,” *Automatica*, vol. 50, no. 10, pp. 2457–2469, 2014.
- [9] J. Schiffer, D. Goldin, J. Raisch, and T. Sezi, “Synchronization of droop-controlled microgrids with distributed rotational and electronic generation,” in *IEEE Conf. on Dec. and Control*, 2013, pp. 2334–2339.
- [10] S. D'Arco and J. A. Suul, “Equivalence of virtual synchronous machines and frequency-droops for converter-based microgrids,” *IEEE Transactions on Smart Grid*, vol. 5, no. 1, pp. 394–395, 2014.
- [11] I. Subotić, D. Groß, M. Colombino, and F. Dörfler, “A lyapunov framework for nested dynamical systems on multiple time scales with application to converter-based power systems,” *IEEE Transactions on Automatic Control*, vol. 66, no. 12, pp. 5909–5924, 2021.
- [12] N. Baeckeland, D. Chatterjee, M. Lu, B. Johnson, and G.-S. Seo, “Overcurrent limiting in grid-forming inverters: A comprehensive review and discussion,” *IEEE Transactions on Power Electronics*, vol. 39, no. 11, pp. 14 493–14 517, 2024.
- [13] Z. Chen, D. Pattabiraman, R. H. Lasseter, and T. M. Jahns, “CERTS microgrids with photovoltaic microsources and feeder flow control,” in *IEEE Energy Conversion Congress and Exposition*, 2016.
- [14] W. Du, R. H. Lasseter, and A. S. Khalsa, “Survivability of autonomous microgrid during overload events,” *IEEE Trans. Smart Grid*, vol. 10, no. 4, pp. 3515–3524, 2019.
- [15] A. Cherukuri, E. Mallada, and J. Cortés, “Asymptotic convergence of constrained primal–dual dynamics,” *Systems & Control Letters*, vol. 87, pp. 10–15, 2016.
- [16] N. Li, C. Zhao, and L. Chen, “Connecting automatic generation control and economic dispatch from an optimization view,” *IEEE Transactions on Control of Network Systems*, vol. 3, no. 3, pp. 254–264, 2016.
- [17] M. Colombino, E. Dall'Anese, and A. Bernstein, “Online optimization as a feedback controller: Stability and tracking,” *IEEE Transactions on Control of Network Systems*, vol. 7, no. 1, pp. 422–432, 2020.
- [18] G. Qu and N. Li, “On the exponential stability of primal-dual gradient dynamics,” *IEEE Control Systems Letters*, vol. 3, no. 1, pp. 43–48, 2019.
- [19] A. Iraniparast and D. Groß, “Networked dynamics with application to frequency stability of grid-forming power-limiting droop control,” *IEEE Transactions on Control of Network Systems*, pp. 1–12, 2025.
- [20] D. Zelazo and M. Mesbahi, “Edge agreement: Graph-theoretic performance bounds and passivity analysis,” *IEEE Trans. Autom. Control*, vol. 56, no. 3, pp. 544–555, 2011.
- [21] J. W. Simpson-Porco, F. Dörfler, and F. Bullo, “Synchronization and power sharing for droop-controlled inverters in islanded microgrids,” *Automatica*, vol. 49, no. 9, pp. 2603–2611, 2013.
- [22] Y. Tang, G. Qu, and N. Li, “Semi-global exponential stability of augmented primal–dual gradient dynamics for constrained convex optimization,” *Systems & Control Letters*, vol. 144, p. 104754, 2020.
- [23] F. Dörfler and F. Bullo, “Kron reduction of graphs with applications to electrical networks,” *IEEE Transactions on Circuits and Systems I: Regular Papers*, vol. 60, no. 1, pp. 150–163, 2013.
- [24] D. P. Bertsekas, *Constrained Optimization and Lagrange Multiplier Methods*, ser. Computer Science and Applied Mathematics. Academic Press, 1982.
- [25] S. Sastry, *Nonlinear Systems: Analysis, Stability, and Control*. Springer-Verlag, 1999.
- [26] S. S. Du and W. Hu, “Linear convergence of the primal-dual gradient method for convex-concave saddle point problems without strong convexity,” in *Proceedings of the Twenty-Second International Conference on Artificial Intelligence and Statistics*, vol. 89, 2019, pp. 196–205.
- [27] A. Tayyebi, D. Groß, A. Anta, F. Kupzog, and F. Dörfler, “Frequency stability of synchronous machines and grid-forming power converters,” *IEEE Journal of Emerging and Selected Topics in Power Electronics*, vol. 8, no. 2, pp. 1004–1018, 2020.
- [28] R. Horn and C. Johnson, *Matrix Analysis*, 2nd ed. Cambridge University Press, 2013.
- [29] F. Bullo, *Lectures on Network Systems*, 1.7 ed., 2024.